the wind-induced upwelling. In the Pacific sector and in coastal regions, strong surface freshening (*26*, *27*) might have caused most of this stabilization, whereas in the lower latitudes of the Atlantic and Indian sectors, warming stabilized the surface waters. The reduction in northward Ekman transport to the lower-latitude Atlantic and Indian sectors during the 2000s (fig. S11), which is probably the result of the zonally more asymmetric atmospheric circulation, also reduced the northward advection of high-latitude waters, lowering the DIC content and/or increasing the alkalinity at the surface.

The trend toward a zonally more asymmetric atmospheric circulation may be related to long-term variations of the tropical sea surface temperature; i.e., to the more prevalent La Niña conditions in the Pacific since the early 2000s (*28*) and the more positive phase of the Atlantic Multidecadal Oscillation over recent decades (*29*). Alternatively, it may be driven by a zonally asymmetric response of the Southern Hemisphere near-surface circulation to the anthropogenic forcing (*25*).

Our results indicate that Earth's most important sink for anthropogenic CO_2 (*5*, *6*) is more variable than previously suggested and that it responds quite sensitively to physical climate variability. This also suggests that should current climate trends reverse in the near future, the Southern Ocean might lose its recently regained uptake strength, leading to a faster accumulation of CO_2 in the atmosphere and consequently an acceleration of the rate of global warming.

REFERENCES AND NOTES

1. C. Le Quéré *et al.*, *Science* **316**, 1735–1738 (2007).
2. N. S. Lovenduski, N. Gruber, *Global Biochem. Cyc.* **22**, GB3016 (2008).
3. A. Lenton *et al.*, *Biogeosciences* **10**, 4037–4054 (2013).
4. C. L. Sabine *et al.*, *Science* **305**, 367–371 (2004).
5. S. E. Mikaloff Fletcher *et al.*, *Global Biogeochem. Cycles* **20**, GB2002 (2006).
6. T. L. Frölicher *et al.*, *J. Clim.* **28**, 862–886 (2015).
7. N. Metzl, *Deep Sea Res. Part II Top. Stud. Oceanogr.* **56**, 607–619 (2009).
8. T. Takahashi *et al.*, *Oceanography* **25**, 26–37 (2012).
9. A. R. Fay, G. A. McKinley, N. S. Lovenduski, *Geophys. Res. Lett.* **41**, 6833–6840 (2014).
10. N. S. Lovenduski, A. R. Fay, G. A. McKinley, *Global Biogeochem. Cyc.* **29**, 416–426 (2015).
11. L. Xue, L. Gao, W.-J. Cai, W. Yu, M. Wei, *Geophys. Res. Lett.* **42**, 3973–3979 (2015).
12. P. Landschützer *et al.*, *Biogeosciences* **10**, 7793–7815 (2013).
13. C. Rödenbeck *et al.*, *Ocean Science* **9**, 193 (2013).
14. C. Rödenbeck, S. Houweling, M. Gloor, M. Heimann, *Atmos. Chem. Phys.* **3**, 1919–1964 (2003).
15. P. Landschützer, N. Gruber, D. C. E. Bakker, U. Schuster, *Global Biogeochem. Cyc.* **28**, 927–949 (2014).
16. P. Landschützer, N. Gruber, D. C. E. Bakker, *A 30 Years Observation-Based Global Monthly Gridded Sea Surface pCO_2 Product from 1982 Through 2011* (Carbon Dioxide Information Analysis Center, Oak Ridge National Laboratory, U.S. Department of Energy, Oak Ridge, TN, 2015).
17. C. Rödenbeck *et al.*, *Biogeosciences* **11**, 4599–4613 (2014).
18. H. D. Graven, N. Gruber, R. Key, S. Khatiwala, X. Giraud, *J. Geophys. Res.* **117**, C10005 (2012).
19. D. C. E. Bakker *et al.*, *Earth System Sci. Data* **6**, 69–90 (2014).
20. D. P. Dee *et al.*, *Q. J. R. Meteorol. Soc.* **137**, 553–597 (2011).
21. A. F. Carril, A. Navarra, *Geophys. Res. Lett.* **28**, 4623–4626 (2001).
22. T. Takahashi *et al.*, *Deep Sea Res. Part II Top. Stud. Oceanogr.* **49**, 1601–1622 (2002).
23. N. Gruber *et al.*, *Global Biogeochem. Cycles* **23**, GB1005 (2009).
24. J. D. Majkut, J. L. Sarmiento, K. B. Rodgers, *Global Biogeochem. Cycles* **28**, 335–351 (2014).
25. F. A. Haumann, D. Notz, H. Schmidt, *Geophys. Res. Lett.* **41**, 8429–8437 (2014).
26. C. De Lavergne, J. B. Palter, E. D. Galbraith, R. Bernardello, I. Marinov, *Nat. Clim. Change* **4**, 278–282 (2014).
27. S. S. Jacobs, C. F. Giulivi, *J. Clim.* **23**, 4508–4524 (2010).
28. Q. Ding, E. J. Steig, D. S. Battisti, M. Küttel, *Nat. Geosci.* **4**, 398–403 (2011).
29. X. Li, D. M. Holland, E. P. Gerber, C. Yoo, *Nature* **505**, 538–542 (2014).

ACKNOWLEDGMENTS

This work was supported by European Union (EU) grant 264879 (CARBOCHANGE) (P.L., N.G., D.C.E.B., M.H., S.v.H., and N.M.) and EU grant 283080 (GEO-CARBON) (P.L. and N.G.), both of which received funding from the European Commission's Seventh Framework Programme. F.A.H. was supporteted by ETH research grant CH2-01 11-1. T.T., R.W., and C.S. acknowledge funding for the pCO_2 from ship projects from the Climate Observation Division of NOAA. T.T. and the Ship of Opportunity Observation Program were supported by a grant (NA10OAR4320143) from NOAA. C.S.'s contribution to this research was made possible by support from the U.S. National Science Foundation's Office of Polar Programs (grants AOAS 0944761 and AOAS 0636975). B.T. was funded through the Antarctic Climate and Ecosystems CRC, the Australian Climate Change Science Program, and the Integrated Marine Observing System. N.M. is grateful for support from the Institut National des Sciences de l'Univers/Centre National de la Recherche Scientifique and the Institut Polaire Française for the Océan Indien Service d'Observation cruises. C.R. thanks the providers of atmospheric CO_2 measurements and the Deutsches Klimarechenzentrum computing center for their support. SOCAT is an international effort, supported by the International Ocean Carbon Coordination Project, the Surface Ocean Lower Atmosphere Study, and the Integrated Marine Biogeochemistry and Ecosystem Research program, to deliver a uniformly quality-controlled surface ocean CO_2 database. The many researchers and funding agencies responsible for the collection of data and quality control are thanked for their contributions to SOCAT. We also thank A. Hogg for fruitful discussions. The surface ocean CO_2 observations are available from the SOCAT website (www.socat.info). The sea surface pCO_2 and air-sea CO_2 flux data leading conclusions of this manuscript are available to the public via the Carbon Dioxide Information Analysis Center (http://cdiac.ornl.gov/oceans/SPCO2_1982_2011_ETH_SOM_FFN.html). The mixed-layer scheme and inversion data supporting the main findings can be obtained from www.bgc-jena.mpg.de/~christian.roedenbeck/download-CO2-ocean/ and www.bgc-jena.mpg.de/~christian.roedenbeck/download-CO2/. P.L. and N.G. designed the study and wrote the paper together with F.A.H. P.L. developed the neural network estimation and performed the majority of the analyses, assisted by F.A.H. C.R. developed the mixed-layer scheme and the atmospheric inversion. S.v.H., M.H., N.M., C.S., T.T., B.T., and R.W. were responsible for the collection of the majority of the surface ocean CO_2 data in the Southern Ocean. D.C.E.B. led the SOCAT synthesis effort that underlies this work. All authors discussed the results and implications and commented on the manuscript at all stages.

SUPPLEMENTARY MATERIALS

www.sciencemag.org/content/349/6253/1221/suppl/DC1
Supplementary Text
Figs. S1 to S12
Tables S1 and S2
References

1 April 2015; accepted 30 July 2015
10.1126/science.aab2620

PLANT SCIENCE

Six enzymes from mayapple that complete the biosynthetic pathway to the etoposide aglycone

Warren Lau and Elizabeth S. Sattely*

Podophyllotoxin is the natural product precursor of the chemotherapeutic etoposide, yet only part of its biosynthetic pathway is known. We used transcriptome mining in *Podophyllum hexandrum* (mayapple) to identify biosynthetic genes in the podophyllotoxin pathway. We selected 29 candidate genes to combinatorially express in *Nicotiana benthamiana* (tobacco) and identified six pathway enzymes, including an oxoglutarate-dependent dioxygenase that closes the core cyclohexane ring of the aryltetralin scaffold. By coexpressing 10 genes in tobacco—these 6 plus 4 previously discovered—we reconstitute the pathway to (−)-4′-desmethylepipodophyllotoxin (the etoposide aglycone), a naturally occurring lignan that is the immediate precursor of etoposide and, unlike podophyllotoxin, a potent topoisomerase inhibitor. Our results enable production of the etoposide aglycone in tobacco and circumvent the need for cultivation of mayapple and semisynthetic epimerization and demethylation of podophyllotoxin.

Although numerous clinically used drugs derive from plant natural products, little is known about their biosynthetic genes, which prevents access to engineered hosts for their production (*1*). Very few complete pathways exist, and only three—artemisinic acid (*2*), the benzylisoquinoline alkaloids (*3*, *4*), and the monoterpenoid indole alkaloids (*5*, *6*)—have been transferred to a heterologous host for current or future industrial production. Knowledge of plant pathways is especially stark in comparison with the >700 bacterial and fungal biosynthetic pathways that have been characterized (*7*).

Podophyllotoxin, a lignan from mayapple, is the natural product precursor to the topoisomerase inhibitor etoposide (*8*–*10*), which is used in dozens of chemotherapy regimens for a variety of malignancies. Although etoposide is on the World Health

Department of Chemical Engineering, Stanford University, Stanford, CA 94305, USA.
***Corresponding author. E-mail: sattely@stanford.edu**

Organization's list of essential medicines, production requires isolation of (–)-podophyllotoxin from the medicinal plant *Podophyllum* (*11*). Subsequent semisynthetic steps to produce etoposide are required for topoisomerase inhibitory activity not present in podophyllotoxin. A complete biosynthetic route would enable more facile access to etoposide and natural and unnatural derivatives that are difficult to produce synthetically (*12*). Early steps of podophyllotoxin biosynthesis (*13*–*16*) involve the unusual enantio- and site-selective dimerization of coniferyl alcohol to form (+)-pinoresinol and provide a starting point for identifying additional biosynthetic genes (Fig. 1). However, biosynthetic gene discovery in *Podophyllum* is a challenge, because the plant grows slowly, the genome is large [~16 Gb (*17*)] and unsequenced, and methods for constructing mutants are laborious (*18*).

We used *Agrobacterium*-mediated transient expression in *N. benthamiana* to test candidate genes for the podophyllotoxin pathway for two reasons. First, this versatile plant host would likely produce correctly folded, active proteins from a variety of enzyme superfamilies without optimization. Second, we wanted to rapidly and combinatorially express candidate enzymes without knowing the order of steps or identities of metabolic intermediates and without additional cloning. Combinatorial expression can be accomplished by coinfiltrating multiple *Agrobacterium* strains—each harboring a different expression construct—and analyzing the resulting plant tissue extracts by using untargeted metabolomics to identify products.

In our initial approach to produce the pathway intermediate (–)-pluviatolide in *N. benthamiana* leaves, we coexpressed three of the four known podophyllotoxin biosynthetic enzymes: pinoresinol-lariciresinol reductase (PLR), secoisolariciresinol dehydrogenase (SDH), and CYP719A23 [dirigent protein (DIR) was not required]. Although we observed low levels of (–)-pluviatolide in the resulting leaf extracts, the amount was insufficient for detecting downstream intermediates produced when coexpressing candidate enzymes (fig. S1). No pluviatolide was detected in control experiments when only green fluorescent protein (GFP) is expressed. To enhance (–)-pluviatolide production *in planta*, we infiltrated leaves expressing CYP719A23 with (–)-matairesinol (isolated from *Forsythia* × *intermedia*) 5 days after *Agrobacterium* infiltration. After 1 day, (–)-pluviatolide concentrations were ~75 times those in leaves expressing PLR, SDH, and CYP719A23, without substrate infiltration (fig. S2), which provided sufficient (–)-pluviatolide to enable candidate enzyme screening.

To select candidate enzymes for conversion of (–)-pluviatolide to the next pathway intermediate, we mined the publicly available *P. hexandrum* RNA-sequencing (RNA-Seq) data set from the Medicinal Plants Consortium. We noted that all known podophyllotoxin genes were highly expressed in rhizome, stem, and leaf tissues, and we selected candidate genes with similar expression profiles (fig. S3). As the order of steps in the pathway was not known, we chose four putative *O*-methyltransferases (*OMT1*–*4*), 12 cytochromes P450 (*CYP*), and a 2-oxoglutarate/Fe(II)-dependent dioxygenase (*2-ODD*). We infiltrated (–)-matairesinol into leaves each coexpressing CYP719A23 and a single candidate enzyme. Liquid chromatography–mass spectrometry (LC-MS) analysis revealed the consumption of (–)-pluviatolide in tobacco leaves coexpressing just one of the candidates, OMT3 (fig. S4). By computationally comparing untargeted metabolomics data from tissue extracts, we identified two compound mass signals unique to CYP719A23 + OMT3 samples relative to CYP719A23 alone: One corresponds to (–)-5′-desmethoxy-yatein (fig. S5); the other, with much lower ion abundance, likely derives from the double methylation of (–)-matairesinol (fig. S6). Expression of OMT3 alone, followed by infiltration of (–)-matairesinol, results in greater amounts of the doubly methylated product, which suggests that this enzyme can accept multiple substrates. We recombinantly expressed OMT3 in *Escherichia coli* and measured its kinetic parameters for (–)-pluviatolide methylation [apparent Michaelis constant (K_m) = 1.4 μM and enzymatic rate (k_{cat}) = 0.72 s^{-1}] (fig. S7). OMT3 accepts (–)-matairesinol and (–)-arctigenin with much lower efficiency and cannot turn over (+)-pinoresinol; these data suggest that OMT3 catalyzes methylation of pluviatolide to generate (–)-5′-desmethoxy-yatein as the next step in the pathway.

We next coexpressed individual candidate CYP and 2-ODD enzymes with CYP719A23 and OMT3; however, we did not observe consumption of (–)-5′-desmethoxy-yatein in leaf extracts, which suggested that our set of candidate genes was incomplete. We reasoned that additional transcriptome data from *P. hexandrum* tissue samples with differential expression of pathway genes could aid candidate selection.

The expression of known (–)-podophyllotoxin biosynthetic genes is up-regulated in *P. hexandrum* leaves after wounding (*19*) (Fig. 2A and fig. S8). LC-MS analysis of metabolites in wounded leaves (removed from the stem to eliminate the possibility of metabolite transport) revealed that both (–)-yatein and (–)-deoxypodophyllotoxin [proposed precursors to (–)-podophyllotoxin (*20*, *21*)] accumulate and reach a maximum level 12 to 24 hours after wounding (fig. S9). Consistent with previous reports (*16*), we did not detect (–)-podophyllotoxin or its glucoside in leaf tissues.

We took advantage of the pathway's inducibility and performed RNA-Seq on triplicate *P. hexandrum* leaf samples, 0, 3, 9, and 12 hours after wounding, from a single plant with the strongest metabolite response. We assembled a leaf transcriptome, determined expression levels, and used predicted enzyme activities required for the missing pathway steps to mine the data for gene sequences encoding *OMT*s, *CYP*s, *2-ODD*s, and polyphenol oxidases (*PPO*s). A computational analysis based on expression profile similarity with

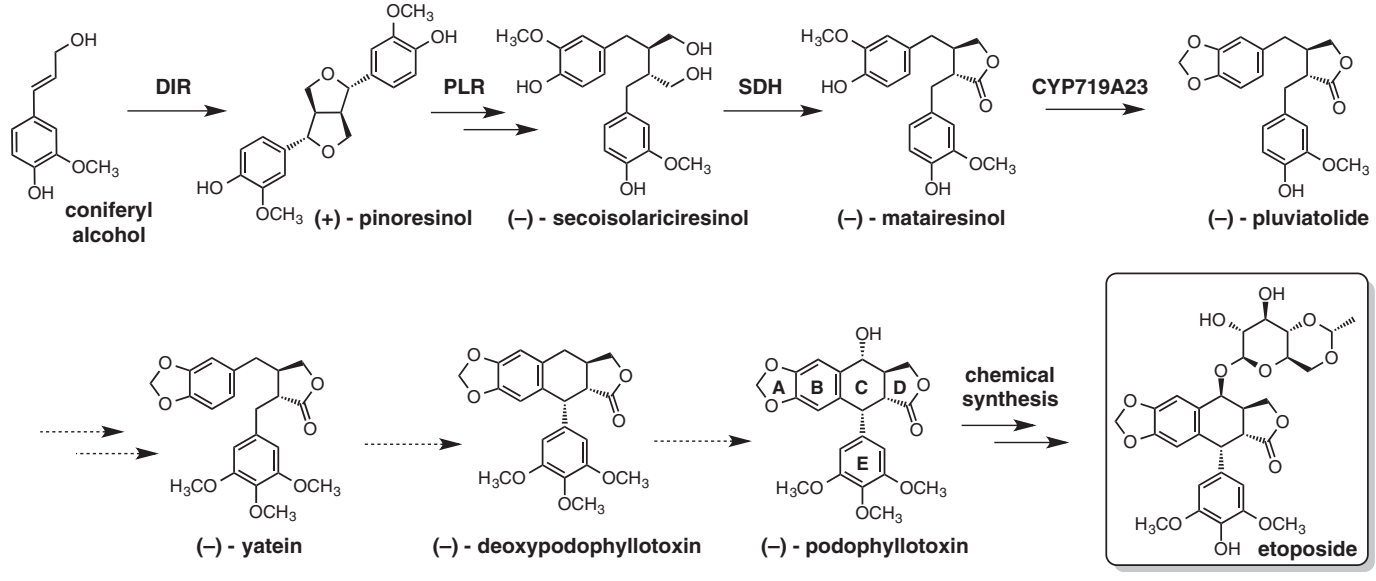

Fig. 1. Biosynthetic pathway of (–)-podophyllotoxin in *P. hexandrum*. Uncharacterized steps are indicated by dashed lines.

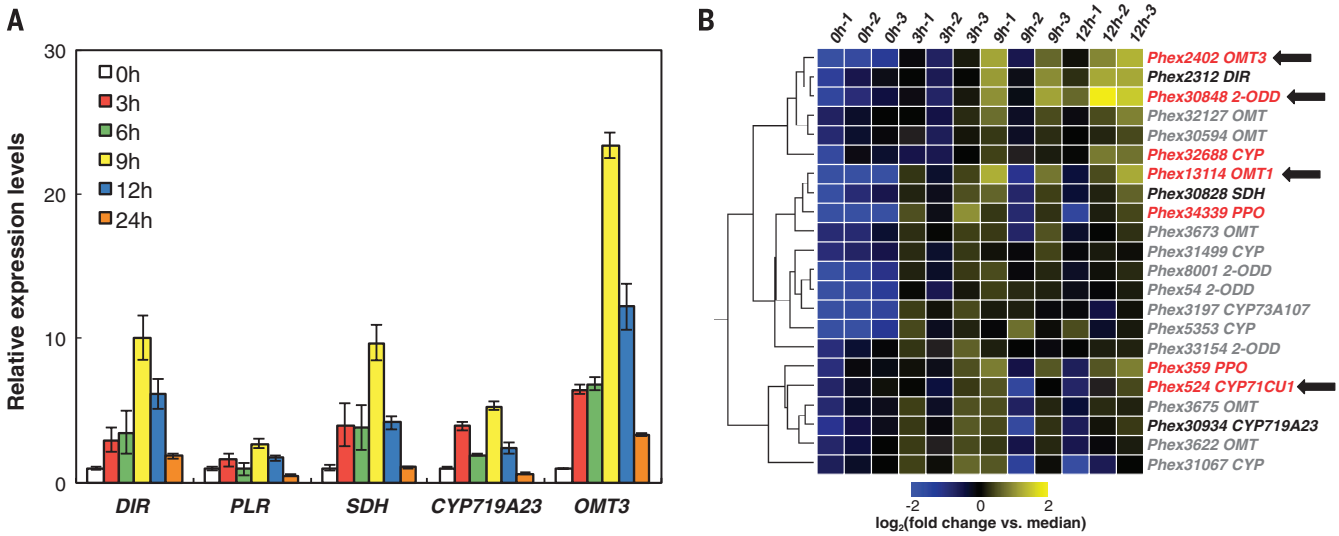

Fig. 2. Expression analysis to identify candidate genes. (**A**) qRT-PCR analysis of podophyllotoxin biosynthetic genes after *P. hexandrum* leaf wounding (at t = 0 hour). Relative expression levels were normalized to t = 0 hour. Data are average values (three technical replicates) ± one SD. (**B**) Hierarchical clustering of RNA-Seq expression data after filtering by enzyme family and expression level. Heat map depicts the expression levels from a single node from the resulting cluster. Color key: Known biosynthetic genes (black), candidate genes (red), genes identified in this report (red with black arrows).

known pathway genes *DIR* and *CYP719A23* and overall expression level yielded seven candidate pathway genes: *Phex30848* (*2-ODD*); *Phex32688* (*CYP*); *Phex13114* (*OMT1*, previously tested); *Phex359* (*PPO*); *Phex34339* (*PPO*); *Phex524* (*CYP71CU1*); and *Phex15199* (*CYP*) (fig. S10 to S12). Hierarchical clustering analysis of 336 expressed genes, selected by filtering all data (34,384 total genes; see table S1) by enzyme family, revealed a single clade of 91 genes; further filtering by expression level condensed this clade to 22 genes containing six of these seven candidates, three of four known pathway genes, and *OMT3* (Fig. 2B).

We individually coexpressed six of these seven candidate enzymes (the putative hydroxylases) with CYP719A23 and OMT3 in tobacco leaves to test for a (–)-5′-desmethoxy-yatein hydroxylase. We infiltrated leaves with (–)-matairesinol 4 days after infiltration and harvested a day later for LC-MS analysis. In samples coexpressing Phex524 (CYP71CU1), we observed turnover of (–)-5′-desmethoxy-yatein (Fig. 3). A comparison of the leaf metabolomes revealed two CYP71CU1-dependent compound mass signals that correspond to the calculated m/z of (–)-5′-desmethyl-yatein [assignment supported by tandem mass spectrometry (MS/MS)] (fig. S13). The earlier eluting mass signal is likely an in-source fragmentation ion originating from a glycosylated derivative of (–)-5′-desmethyl-yatein produced by endogenous tobacco enzymes. Thus, CYP71CU1 likely catalyzes the next pathway step as part of E-ring functionalization.

To complete the biosynthesis of (–)-yatein, a proposed intermediate in the podophyllotoxin pathway (*21*), we tested Phex13114 (OMT1) for the ability to methylate (–)-5′-desmethyl-yatein. We infiltrated (–)-matairesinol into tobacco leaves expressing OMT1 in combination with CYP719A23, OMT3, and CYP71CU1. (–)-5′-Desmethyl-yatein could not be detected in leaf extracts in which OMT1 had been coexpressed (Fig. 3 and fig. S14); instead, we detected the accumulation of (–)-yatein. Thus, OMT1 likely converts (–)-5′-desmethylyatein to (–)-yatein as the seventh step in the pathway.

The remainder of the pathway involves closing the central six-membered ring in the aryltetralin scaffold and oxidative tailoring. In our initial screen (coexpression with CYP719A23 and OMT3), we observed substantial consumption of (–)-5′-desmethoxy-yatein in samples coexpressing Phex30848 (2-ODD). Computational comparison of leaf metabolomes revealed a new 2-ODD–dependent compound mass signal that corresponds to 5′-desmethoxy-deoxypodophyllotoxin bearing the required aryltetralin scaffold (assignment supported by MS/MS analysis) (fig. S14). We hypothesize that the reaction mechanism involves activation of the 7′ carbon by hydroxylation, followed by dehydration and carbon-carbon bond formation via a quinone methide intermediate (fig. S16).

Prior feeding studies (*21*) and our *P. hexandrum* wounding metabolomics data suggest that (–)-yatein is the native substrate for ring closure. Therefore, we tested whether 2-ODD could also catalyze the conversion of (–)-yatein to (–)-deoxypodophyllotoxin *in planta*. We expressed 2-ODD in tobacco leaves along with CYP719A23, OMT3, CYP71CU1, and OMT1. Four days after *Agrobacterium* infiltration, we infiltrated leaves with (–)-matairesinol and, a day later, harvested them for LC-MS analysis. We observed that (–)-yatein was consumed in a 2-ODD–dependent fashion, and a computational comparison of metabolite extracts confirmed the accumulation of (–)-deoxypodophyllotoxin in tobacco leaves coexpressing 2-ODD (Fig. 3 and fig. S17). Thus 2-ODD catalyzes oxidative ring closure to establish the core of the aryltetralin scaffold.

We sought to confirm the activities of these enzymes by biochemical analysis. We isolated microsomes enriched with Phex524 (CYP71CU1) after expression in *Saccharomyces cerevisiae WAT11*, and purified Phex13114 (OMT1) and Phex30848 (2-ODD) with C-terminal hexahistidine tags after expression in *E. coli*. As expected, incubation of (–)-5′-desmethoxy-yatein with CYP71CU1 and the reduced form of nicotinamide adenine dinucleotide phosphate (NADPH) gave the hydroxylated product, (–)-5′-desmethyl-yatein; incubation with CYP71CU1 and OMT1, and with the cofactors, NADPH and *S*-adenosylmethionine, gave (–)-yatein (fig. S18). Incubation of 2-ODD with (–)-yatein as the substrate in the presence of 2-oxoglutarate and Fe^{2+} yielded (–)-deoxypodophyllotoxin. All enzymes showed little to no activity on similar substrates under identical assay conditions. These data confirm the enzyme activities and order of reactions for the pathway through (–)-deoxypodophyllotoxin (Fig. 3 and fig. S19).

To identity the enzyme involved in what we hypothesized to be the final step of (–)-podophyllotoxin biosynthesis, the hydroxylation of (–)-deoxypodophyllotoxin, we returned to the publicly available transcriptome data to identify *CYPs* predominantly and highly expressed in *P. hexandrum* rhizomes, the tissue in which (–)-podophyllotoxin is primarily produced. We identified six *CYP* candidates that matched our criterion (fig. S20). We screened the candidates in tobacco by individual coexpression with the five (–)-deoxypodophyllotoxin biosynthetic genes, starting from CYP719A23 and infiltration of (–)-matairesinol. By a comparative metabolomic analysis, we observed consumption of (–)-deoxypodophyllotoxin in leaves coexpressing the candidate enzyme, Ph14372 (CYP71BE54), but—contrary to our expectation—no (–)-podophyllotoxin was detected (Fig. 3). Instead, we observed CYP71BE54-dependent accumulation of two compound mass signals with predicted molecular formulas and MS/MS data that correlate to

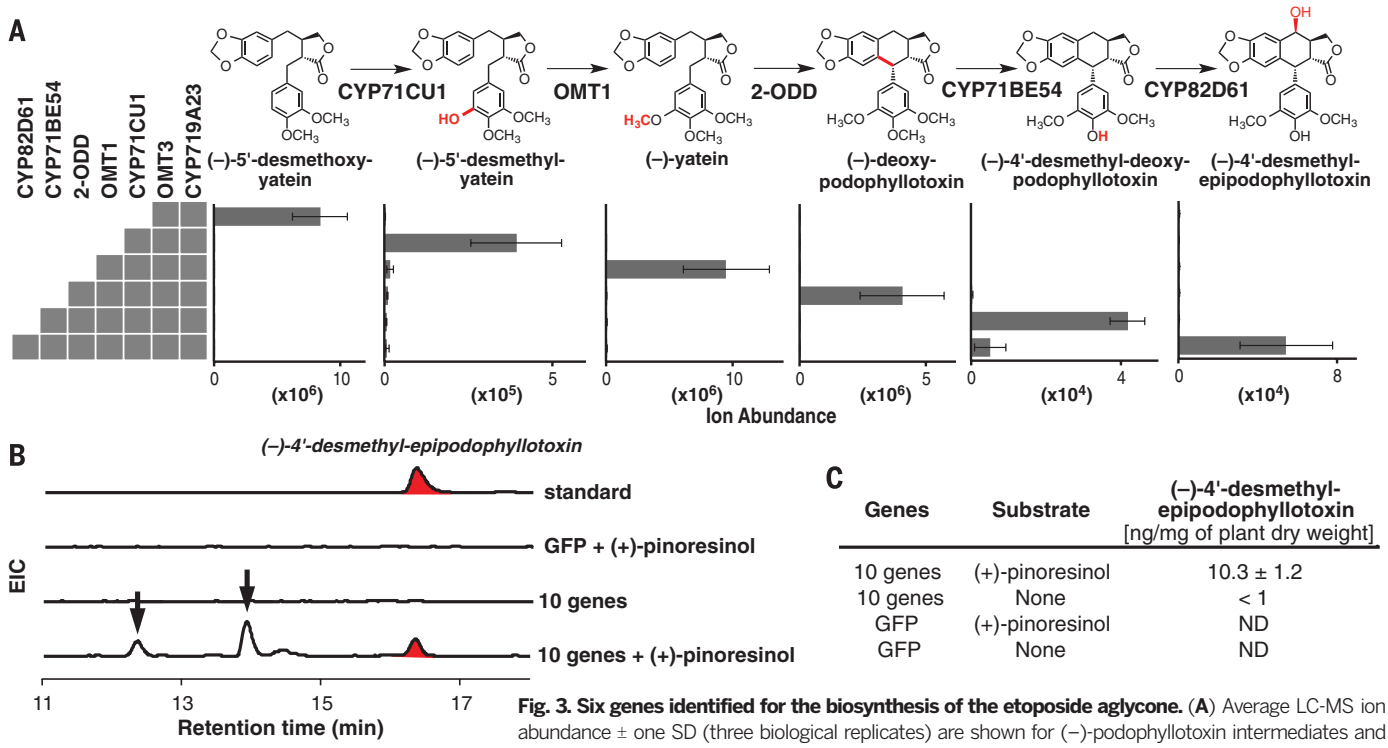

Genes	Substrate	(–)-4'-desmethyl-epipodophyllotoxin [ng/mg of plant dry weight]
10 genes	(+)-pinoresinol	10.3 ± 1.2
10 genes	None	< 1
GFP	(+)-pinoresinol	ND
GFP	None	ND

Fig. 3. Six genes identified for the biosynthesis of the etoposide aglycone. (**A**) Average LC-MS ion abundance ± one SD (three biological replicates) are shown for (–)-podophyllotoxin intermediates and derivatives produced in tobacco after expression of indicated enzymes and (–)-matairesinol infiltration. (**B**) Extracted ion chromatograms (EIC) for the etoposide aglycone, (–)-4′-desmethylepipodophyllotoxin (*m/z* = 401) in tobacco leaves expressing GFP or DIR, PLR, SDH, CYP719A23, and the six genes identified in this report with and without the infiltration of (+)-pinoresinol. Arrows indicate glycosylated derivatives of (–)-4′-desmethylepipodophyllotoxin. (**C**) Average amounts of (–)-4′-desmethylepipodophyllotoxin detected in tobacco ± one SD (three biological replicates).

compounds derived from the demethylation of (–)-deoxypodophyllotoxin, formally (–)-4′-desmethyl-deoxypodophyllotoxin (fig. S21). The earlier eluting mass signal is likely derived from a glycosylated derivative. The observed activity of CYP71BE54 implies that the demethylated lignans found in *P. hexandrum* (*22*–*24*) are a result of enzymatic demethylation rather than the failure of OMT3 to methylate a portion of the lignan flux. Consistent with this view, CYP71CU1-enriched microsomes cannot accept (–)-pluviatolide as a substrate, which indicates a need for fully methylated substrate earlier in the pathway. Despite poor expression in yeast, isolated CYP71BE54 microsomes accepted (–)-deoxypodophyllotoxin as a substrate but not other similar molecules (fig. S22).

Upon screening an additional candidate P450, *Ph35407* (*CYP82D61*), we also observed consumption of (–)-deoxypodophyllotoxin. However, we did not detect formation of (–)-podophyllotoxin; instead, we observed accumulation of its epimer, (–)-epipodophyllotoxin (fig. S23). To confirm the activity of CYP82D61 in the context of the late pathway enzymes, we infiltrated (–)-matairesinol into tobacco leaves expressing CYP71BE54, CYP82D61, and the five (–)-deoxypodophyllotoxin biosynthetic genes starting from CYP719A23. Comparative metabolomics demonstrated the accumulation of (–)-4′-desmethylepipodophyllotoxin, along with two other earlier eluting compound mass signals that are likely derived from glycosylated (–)-4′-desmethylepipodophyllotoxin derivatives (Fig. 3 and fig. S24). (–)-4′-Desmethylepipodophyllotoxin is the direct precursor to etoposide, which currently is made by chemical modification of podophyllotoxin. Potent topoisomerase activity of etoposide was discovered by serendipitous derivatization of trace amounts of (–)-4′-desmethyl-epipodophyllotoxin glucoside, present in *P. hexandrum* rhizome extracts (*8*).

Having discovered six enzymes that complete the pathway to (–)-4′-desmethylepipodophyllotoxin, we then sought to reconstitute the pathway in *N. benthamiana* from (+)-pinoresinol. We expressed DIR, PLR, SDH, CYP719A23, and the six enzymes that we identified in tobacco leaves and subsequently infiltrated 100 μM (+)-pinoresinol, yielding 10.3 ng of (–)-4′-desmethylepipodophyllotoxin per mg of plant dry weight. The total amount produced is likely even higher, as some of the product is derivatized by tobacco enzymes and could not be quantified. Less than 1 ng of product per mg of plant dry weight was obtained without infiltration of (+)-pinoresinol, which suggested that native production of this intermediate in tobacco is limiting (Fig. 3, B and C). We also produced (–)-deoxypodophyllotoxin and (–)-epipodophyllotoxin starting from (+)-pinoresinol in *N. benthamiana* by omitting CYP71BE54 and CYP82D61, and CYP71BE54, respectively (figs. S25 and S26); pathway intermediates do not accumulate in either case (fig. S27). The yield of (–)-deoxypodophyllotoxin in tobacco (~90 ng/mg dry weight) is more than one-third of the yield from wound-induced leaves of *Podophyllum*.

Thus, the etoposide aglycone, (–)-4′-desmethyl-epipodophyllotoxin, can be produced in *N. benthamiana*, which circumvents the current need for mayapple cultivation and subsequent semisynthetic epimerization and demethylation (fig. S28). By coupling transcriptome mining with combinatorial expression of candidate enzymes in tobacco, we identified six biosynthetic enzymes, including a 2-ODD that catalyzes the novel C-C bond-forming step for stereoselective cyclization to close the aryltetralin scaffold and a late-stage P450 to unmask the E-ring phenol. A similar approach could be used to engineer synthetic pathways that produce podophyllotoxin derivatives with improved bioactive properties.

REFERENCES AND NOTES

1. V. De Luca, V. Salim, S. M. Atsumi, F. Yu, *Science* **336**, 1658–1661 (2012).
2. C. J. Paddon *et al.*, *Nature* **496**, 528–532 (2013).
3. K. Thodey, S. Galanie, C. D. Smolke, *Nat. Chem. Biol.* **10**, 837–844 (2014).
4. W. C. DeLoache *et al.*, *Nat. Chem. Biol.* **11**, 465–471 (2015).
5. S. Brown, M. Clastre, V. Courdavault, S. E. O'Connor, *Proc. Natl. Acad. Sci. U.S.A.* **112**, 3205–3210 (2015).
6. Y. Qu *et al.*, *Proc. Natl. Acad. Sci. U.S.A.* **112**, 6224–6229 (2015).
7. P. Cimermancic *et al.*, *Cell* **158**, 412–421 (2014).
8. H. F. Stähelin, A. von Wartburg, *Cancer Res.* **51**, 5–15 (1991).
9. C. Canel, R. M. Moraes, F. E. Dayan, D. Ferreira, *Phytochemistry* **54**, 115–120 (2000).
10. M. Gordaliza, P. A. García, J. M. Miguel del Corral, M. A. Castro, M. A. Gómez-Zurita, *Toxicon* **44**, 441–459 (2004).
11. H. Lata, C. S. Mizuno, R. M. Moraes, in *Protocols for in Vitro Cultures and Secondary Metabolite Analysis of Aromatic and Medicinal Plants* (Springer, 2009), pp. 387–402.
12. A. Kamal, S. M. Ali Hussaini, A. Rahim, S. Riyaz, Podophyllotoxin derivatives: A patent review (2012–2014). *Expert Opin. Ther. Patents* 10.1517/13543776.2015.1051727 (2015).
13. A. T. Dinkova-Kostova *et al.*, *J. Biol. Chem.* **271**, 29473–29482 (1996).
14. L. B. Davin *et al.*, *Science* **275**, 362–367 (1997).

15. Z.-Q. Xia, M. A. Costa, H. C. Pélissier, L. B. Davin, N. G. Lewis, *J. Biol. Chem.* **276**, 12614–12623 (2001).
16. J. V. Marques *et al.*, *J. Biol. Chem.* **288**, 466–479 (2013).
17. A. Nag, S. Chanda, R. Subramani, *J. Cell Plant Sci.* **2**, 19–23 (2011).
18. M. Rajesh *et al.*, *Plant Cell Tissue Organ Cult.* **114**, 71–82 (2013).
19. D. P. Wankhede, D. K. Biswas, S. Rajkumar, A. K. Sinha, *Protoplasma* **250**, 1239–1249 (2013).
20. W. M. Kamil, P. M. Dewick, *Phytochemistry* **25**, 2089–2092 (1986).
21. W. M. Kamil, P. M. Dewick, *Phytochemistry* **25**, 2093–2102 (1986).
22. A. J. Broomhead, M. M. A. Rahman, P. M. Dewick, D. E. Jackson, J. A. Lucas, *Phytochemistry* **30**, 1489–1492 (1991).
23. D. E. Jackson, P. M. Dewick, *Phytochemistry* **23**, 1147–1152 (1984).
24. D. E. Jackson, P. M. Dewick, *Phytochemistry* **23**, 1037–1042 (1984).

ACKNOWLEDGMENTS

This work was supported by the NIH grants R00 GM089985 and DP2 AT008321 (E.S.S.). We thank J. Rajniak, A. P. Klein, and M. Voges (Stanford) for critical reading of the manuscript, and members of the Sattely lab for helpful discussions. We thank J.-G. Kim (Stanford) for assistance with *N. benthamiana* transient expression, quantitative reverse transcription polymerase chain reactions (qRT-PCR) and RNA-Seq library preparation, G. Lomonossoff (John Innes Centre) for plasmid pEAQ, and D. Nelson for CYP nomenclature assignment. We thank the Stanford Center for Genomics and Personalized Medicine for RNA sequencing services and the Stanford Genetics Bioinformatics Service Center for computational resources. Gene sequences have been deposited into GenBank (accession numbers: KT390155 to KT390182). RNA Sequencing data have been deposited into the National Center for Biotechnology Information, NIH, Sequence Read Archive (accession number: SRP061783). E.S.S., W.L., and Stanford University have filed a provisional patent application. Supplementary materials contain additional data.

SUPPLEMENTARY MATERIALS

www.sciencemag.org/content/349/6253/1224/suppl/DC1
Materials and Methods
Figs. S1 to S38
Tables S1 and S2
References (*25*–*51*)

3 June 2015; accepted 22 July 2015
10.1126/science.aac7202

ANTIVIRAL IMMUNITY

Viruses transfer the antiviral second messenger cGAMP between cells

A. Bridgeman,[1] J. Maelfait,[1] T. Davenne,[1] T. Partridge,[2] Y. Peng,[1] A. Mayer,[1] T. Dong,[1] V. Kaever,[3] P. Borrow,[2] J. Rehwinkel[1]*

Cyclic GMP–AMP synthase (cGAS) detects cytosolic DNA during virus infection and induces an antiviral state. cGAS signals by synthesis of a second messenger, cyclic GMP-AMP (cGAMP), which activates stimulator of interferon genes (STING). We show that cGAMP is incorporated into viral particles, including lentivirus and herpesvirus virions, when these are produced in cGAS-expressing cells. Virions transferred cGAMP to newly infected cells and triggered a STING-dependent antiviral program. These effects were independent of exosomes and viral nucleic acids. Our results reveal a way by which a signal for innate immunity is transferred between cells, potentially accelerating and broadening antiviral responses. Moreover, infection of dendritic cells with cGAMP-loaded lentiviruses enhanced their activation. Loading viral vectors with cGAMP therefore holds promise for vaccine development.

Type I interferons (IFNs) play pivotal roles in the immune response to virus infection (*1*). IFN expression is induced by signaling pathways activated by sensors of virus presence, including cytosolic DNA sensors (*2*, *3*). Cyclic GMP–AMP synthase (cGAS) is a cytosolic DNA sensor that signals by catalyzing the synthesis of a second messenger, cyclic GMP-AMP (cGAMP) (*4*, *5*). cGAMP binds to and activates stimulator of interferon genes (STING) (*5*, *6*), which plays a central role in cytosolic DNA sensing by relaying signals from DNA sensors to transcription factors driving *IFN* gene transcription (*3*, *7*).

DNA viruses and retroviruses trigger cGAS-dependent IFN responses in infected cells (*8*–*15*). This is thought to involve sensing by cGAS of viral DNA, leading to *IFN* gene transcription in the same cell where DNA detection occurred or in neighboring cells connected by gap junctions (*16*). However, it is conceivable that IFN induction upon virus infection could also occur independently of cGAS if the infecting virus were to incorporate and transfer the cGAMP second messenger. For example, human immunodeficiency virus 1 (HIV-1) particles incorporate host molecules such as APOBEC3G (*17*). Given this precedent, we hypothesized that cGAMP can be packaged into virions and elicits an IFN response in newly infected cells independently of cGAS expression by the latter, allowing for potentiation of innate antiviral immunity.

To test this idea, we produced HIV-1–based lentiviral vectors by plasmid transfection in 293T cells, a human cell line that does not express cGAS (*4*). Virus particles were pseudotyped with vesicular stomatitis virus glycoprotein (VSV-G), and the viral genome contained enhanced green fluorescent protein (EGFP) in the *Env* open reading frame. These viruses, henceforth referred to as HIV-1-GFP, are replication incompetent due to the lack of functional *Env*. Some 293T cells were cotransfected with expression constructs for either wild-type mouse cGAS (m-cGAS) or catalytically inactive m-cGAS-G198A/S199A (m-cGAS-AA) (*4*). Titrated virus stocks were then used to infect fresh human embryonic kidney 293 (HEK293) cells, which express endogenous STING (*7*, *18*) and induce IFN in response to cGAMP (fig. S1, A to D). HIV-1-GFP collected from cGAS-expressing cells triggered induction of an *IFN*β promoter reporter, whereas viruses produced in the absence of exogenous cGAS or in the presence of mutant cGAS did not (Fig. 1A). Next, we analyzed IFN secretion by transferring supernatants from infected cells to a reporter cell line (HEK293-ISRE-luc), in which firefly luciferase expression is driven by interferon-stimulated response elements (ISREs) (fig. S1E). Only virus stocks produced in wild-type cGAS-expressing cells triggered IFN secretion (fig. S1F). Moreover, infected cells induced *IFI44* and *IFIT1* mRNAs specifically when cGAS was present in virus producer cells, further demonstrating induction of interferon-stimulated genes (ISGs) (fig. S1G). We made similar observations when infecting the myeloid cell line THP1 (fig. S2). Next, we infected primary mouse bone marrow–derived macrophages (BMDMs). IFN and ISGs were induced in BMDMs that had been infected with HIV-1-GFP produced in cGAS-reconstituted 293T cells (Fig. 1, B and C). STING-deficient BMDMs did not induce IFN and ISGs in response to the same virus preparations, although retinoic acid–inducible gene I (RIG-I)–dependent IFN production triggered by Sendai virus (SeV) was normal (Fig. 1, B and C). The increased IFN production triggered by HIV-1–GFP was functionally relevant, because infection with HIV-1-GFP produced in the presence of cGAS conferred a STING-dependent antiviral state against subsequent challenge with encephalomyocarditis virus (EMCV) or herpes simplex virus 1 (HSV-1) (Fig. 1D).

To exclude the possibility that transfer of plasmid DNA or of a soluble factor accounts for IFN production by freshly infected cells, we treated virus preparations with deoxyribonuclease or pelleted virions by centrifugation. Neither treatment affected the ability of HIV-1-GFP produced in cGAS-expressing cells to induce IFN (fig. S3, A and B). The IFN response in target cells was independent of reverse transcription and integration, as shown by pharmacological inhibition with nevirapine and raltegravir, respectively (fig. S3C). Virus-like particles lacking the viral RNA genome induced IFN in target cells when collected from cGAS-expressing producer cells (fig. S3D). These observations demonstrate that neither the viral genome nor its reverse transcription products account for IFN

[1]Medical Research Council Human Immunology Unit, Medical Research Council Weatherall Institute of Molecular Medicine, Radcliffe Department of Medicine, University of Oxford, Oxford OX3 9DS, UK. [2]Nuffield Department of Medicine, University of Oxford, Oxford OX3 7FZ, UK. [3]Research Core Unit Metabolomics, Institute of Pharmacology, Hannover Medical School, Carl-Neuberg-Strasse 1, D-30625 Hannover, Germany.
***Corresponding author. E-mail: jan.rehwinkel@imm.ox.ac.uk**

Six enzymes from mayapple that complete the biosynthetic pathway to the etoposide aglycone

Warren Lau and Elizabeth S. Sattely

Science **349** (6253), 1224-1228.
DOI: 10.1126/science.aac7202

Transplanting the wisdom of the mayapple

Etoposide, a topoisomerase inhibitor, is used to treat various cancers. However, etoposide isn't that easy to get. Its precursor comes from the very slow-growing mayapple plant. Lau and Sattely used bioinformatics, heterologous enzyme expression, and kinetic characterization, to work out the pathway that makes the precursor in mayapple (see the Perspective by O'Connor). They then successfully transplanted the full biosynthetic pathway into tobacco plants.

Science, this issue p. 1224; see also p. 1167